Journal of Materials Research and Technology 29 (2024) 5252–5258

Contents lists available at ScienceDirect

Journal of Materials Research and Technology

journal homepage: www.elsevier.com/locate/jmrt

Atomic-scale characterization of V-shaped interface structure of η_1 precipitates in Al–Zn–Mg alloy

Hwangsun Kim [a], Juhyun Oh [a], Young-Kyun Kwon [b], Howook Choi [a], Siwhan Lee [a], Byeongjun Gil [a], Eun Soo Park [a], Miyoung Kim [a], Heung Nam Han [a,*]

[a] Department of Materials Science and Engineering & Research Institute of Advanced Materials, Seoul National University, Seoul, 08826, Republic of Korea
[b] Department of Physics, Department of Information Display, and Research Institute for Basic Sciences, Kyung Hee University, Seoul, 02447, Republic of Korea

ARTICLE INFO

Keywords:
Aluminum alloy
Precipitation
Interface structure
Transmission electron microscopy (TEM)
First-principles calculation

ABSTRACT

Al–Zn–Mg alloys have attracted significant interest in the automotive industry owing to their high strength and light weight. Precipitation hardening is the primary mechanism by which these alloys are strengthened, meaning the analysis of the shape, size, and fraction of the precipitates is crucial. In this study, the interfacial structure of precipitates, which influences the mechanical properties of alloys, was investigated. Aberration-corrected scanning transmission electron microscopy studies revealed the atomic structure of the unique V-shaped interface structure of the η_1 precipitates, which are the most prevalent among the η precipitates produced in this alloy. The structure was investigated from an energetic perspective using first-principles calculations, which revealed that the formation of the V-shaped interface structure increased the stability through strain relaxation in both the aluminum matrix and η_1. The results provide valuable insights into the formation and growth mechanisms of precipitates, paving the way for further advancements in this field.

1. Introduction

Advancements in the transportation and mobility sectors increasingly rely on the development of lightweight alloys, known for their exceptional strength-to-weight ratios, to enhance fuel efficiency [1–6]. Among the many lightweight alloys available, aluminum and magnesium alloys are notable for their favorable mechanical properties. Aluminum–zinc–magnesium (Al–Zn–Mg) alloys, also known as the aluminum alloy 7xxx series (AA 7xxx series), have gained considerable attention owing to their high strength. Furthermore, the AA 7000 series alloys are highly attractive candidates for industrial applications owing to the cost-effectiveness of the constituent elements, aluminum, magnesium, and zinc. Precipitation hardening has been identified as a key factor in achieving a remarkable ultimate tensile strength, and strengths above 700 MPa, the highest among all aluminum alloys, have been achieved using this technique [7,8]. The mechanical properties of these alloys are intricately linked to the morphology, size, and distribution of precipitates formed during this process. Thus, a detailed understanding of precipitate characteristics, especially their interfacial structures, is crucial for comprehensively understanding the AA 7000 series alloys' mechanical behavior.

Various types of η' and η are considered representative precipitates of the Al–Zn–Mg alloys. The evolution of η precipitates has been extensively examined [9–16], universally follows the transformation from a super saturated solid solution (s.s.s.s.) → Guinier Preston (GP) zones → η' → η ($MgZn_2$). This sequence can also progress directly from s.s.s.s.→$GP_{\eta p}$→η_p→η (MgZn2). Among the GP zones, GP I and GP II have been distinguished in Al–Zn–Mg alloys [14]. GP I zones, emerging from solute-rich clusters between room temperature and 150 °C, display a spherical morphology [12,14,17,18]. Conversely, GP II zones, originating from vacancy-rich clusters in the $(111)_{Al}$ habit plane, necessitate a high vacancy concentration for formation which can be achieved by quenching at 450 °C or higher and aging at 70 °C or higher. Recent in situ transmission electron microscopy (TEM) investigations have identified the GP I/aluminum interface acts as a nucleation site for GP II zones [19].

The plate-like morphology of η′ with a hexagonal structure and space group $P6_3/mmc$ has been extensively characterized [20–24]. This structure transitions into η, resembling the C14 Laves phase polytype (a = b = 0.522 nm, c = 0.857 nm) with the same space group $P6_3/mmc$. Research has identified fifteen distinct η precipitate types with varying orientation relationships with the aluminum matrix, with η_1, η_2, and η_4

* Corresponding author.
E-mail address: hnhan@snu.ac.kr (H.N. Han).

https://doi.org/10.1016/j.jmrt.2024.03.012
Received 18 December 2023; Received in revised form 7 February 2024; Accepted 1 March 2024
Available online 3 March 2024

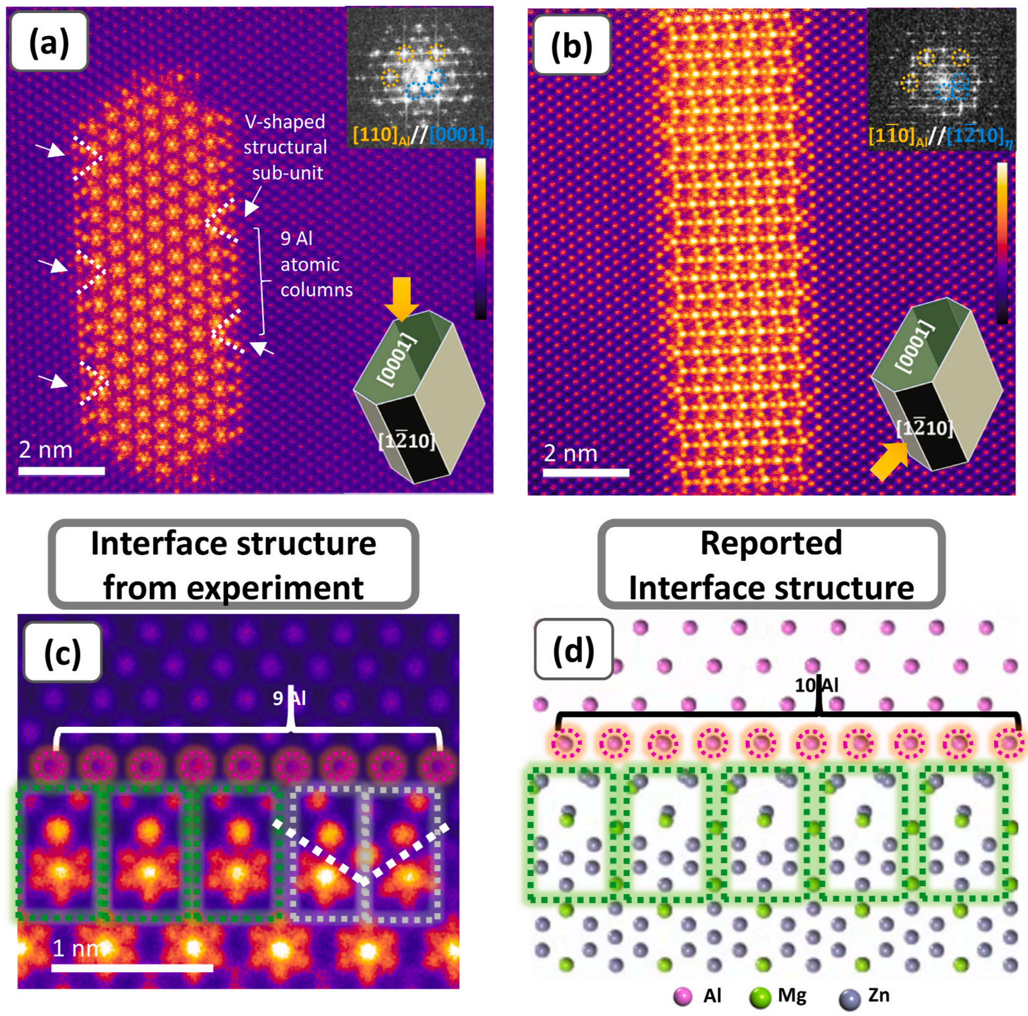

Fig. 1. HAADF-STEM images of η_1 along different zone axis: (a) $[110]_{Al}//[0001]_\eta$ (b) $[1\ \bar{1}\ 0]_{Al}//[1\ \bar{2}\ 10]_\eta$. Yellow directions indicate the observed plane of η_1 precipitate. (c) Experimentally observed interface structure of η_1. (d) Previously reported [28] interface structure of η_1 without consideration of V-shaped structural sub-unit. (For interpretation of the references to color in this figure legend, the reader is referred to the Web version of this article.)

being the most commonly observed types in over-aged Al–Zn–Mg alloys [25–28]. Notably, η_1 precipitate constitutes up to 50 % of precipitates in over-aged 7003 alloy [29,30]. The formation mechanism of η_1 remains controversial, with some studies suggesting that η_1 nucleates from pre-existing GP zones, whereas others propose that it precipitates directly out of the solid solution without the aid of any transition phases [22,31,32]. Recent studies have shed light on the formation pathway of η_1 via the metastable phase η', and the interface structure of η_1 has been revealed using aberration-corrected TEM and first-principles calculations [30,33]. The co-segregation of magnesium and zinc atoms at the planar η_1/aluminum matrix interface has been reported suggesting vacancies along this interface [30,33]. Both studies reported the periodic distribution of sub-unit structures. A recent study reported that precipitates with unique step-like interface structure could be energetically favored compared to the precipitates having planar interface structure due to the strain relief effect [34,35]. Moreover, interface of Al/η can also act as hydrogen trap site, performing as crack initiation source that affects the mechanical property [36,37]. The distinct interface structure of η_1, particularly its unique sub-units, may be the reason why it can occupy a larger proportion than other precipitates and may affect the mechanical property, but the precise interface structure and the role of the unique sub-units have not been elucidated at the atomic scale.

In this study, we conducted a comprehensive structural characterization of η_1 precipitate interfaces, employing aberration corrected scanning TEM (STEM), first-principles calculations, and STEM image simulations. We focused specifically on the structural sub-unit at the interface of η_1, the most prevalent η precipitate form. The findings of this study offer novel insights into the growth mechanism related to the interface structure and provide a pathway for controlling the precipitation kinetics to tailor the mechanical properties of the alloys.

2. Methods

The Al–5Zn-1.5 Mg alloy was fabricated via vacuum induction melting to eliminate the confounding effects of other alloying elements on the formation of η precipitates. Small samples were extracted from the ingots and subjected to homogenization at 460 °C for 24 h, followed by quenching in water at room temperature and cold rolling into sheets measuring 0.5 mm in thickness. The sheets were subsequently solution-treated at 460 °C for 1 h and quenched in water, leading to the formation of η precipitates after pre-aging at 100 °C for approximately 5 h and aging at 150 °C for approximately 6 h. To prepare thin TEM specimens, discs of 3 mm diameter were sectioned from the sheets and thinned mechanically to 0.07 mm before being subjected to twin-jet electropolishing at −25 °C and a working voltage of 11 V. The electrolyte was composed of 33% nitric acid and 67% methanol.

High-angle annular dark-field scanning TEM (HAADF-STEM) images were acquired using a Cs-corrected Thermo Fisher Themis Z and the

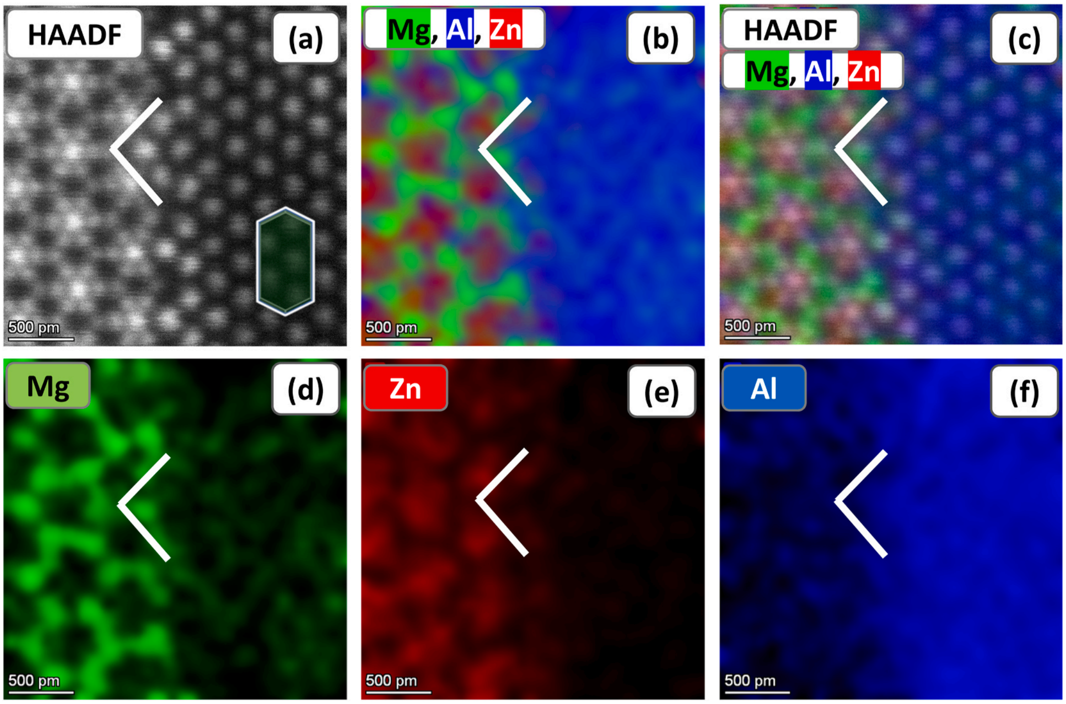

Fig. 2. Atomic scale EDS analysis results of η_1/Al interface. White lines indicate V-shaped sub-unit interface structure. (a) HAADF map (b) Combination of Al, Zn and Mg map (c) Combination of HAADF, Al, Zn and Mg map (d) Mg map (e) Zn map (f) Al map.

energy-dispersive X-ray spectroscopy (EDS) images were obtained at 200 kV. The convergence semi-angle and inner collection angles were 30 and 50 mrad, respectively. STEM simulations were performed at 200 kV using Dr. Probe software [38]. Spherical aberration coefficients of Cs = 0 mm, C5 = 0 mm, and C7 = 0 mm without astigmatism, a convergence semi-angle of 30 mrad, and a slice thickness of 8 Å were used during the simulations. The thickness of each specimen was set to 40 nm.

First-principles calculations were performed using the Vienna Ab initio Simulation Package. A projector-augmented wave method with local density approximation was used. For all calculations, an energy cut-off of 400 eV was used for the plane-wave basis set expansion. The atomic model size of planar interface model was a = 4.21 Å, b = 8.22 Å, and c = 38.74 Å with total atom number of 159. The atomic model size of sub-unit interface structure model was a = 25.54 Å, b = 8.49 Å, and c = 29.88 Å with total atom number of 249. $[0001]_\eta$ direction and [12 10]η direction were set as x and y directions for planar interface model sampling and y and x directions sub-unit interface structure model sampling, respectively. In case of sub-unit interface structure model, a vacuum layer minimum of >10 Å was employed. The K-points were set to 6 × 4 × 1 for the planar interface model and 1 × 4 × 1 for the sub-unit interface structure model based on the Monkhorst-Pack scheme. Gaussian smearing with 0.2 eV width of smearing was used for smearing parameters. For the optimization, we used residual minimization method direct inversion algorithm. The ground-state atomic structures were obtained by minimizing the Hellman-Feynman forces until the total forces on each ion converged within 0.02 eV/Å.

3. Results and discussion

3.1. Atomic structure characterization of η_1 interface structure

The atomic structure of the η_1 precipitates was examined using HAADF-STEM, leveraging the orientation relationship of $[0001]_\eta$// $[110]_{Al}$ with $(0\,\bar{1}\,10)_\eta//(001)_{Al}$ and $[1\,\bar{2}\,10]_\eta//[1\,\bar{1}\,0]_{Al}$ with $(10\,\bar{1}\,0)_\eta$// $(001)_{Al}$ for direct observations of $[0001]_\eta$ and $[1\ \bar{2}\ 10]_\eta$ along the $<110>_{Al}$ zone axis (Fig. 1(a) and (b)). This analysis revealed the distinctive hexagonal and elongated rectangular morphologies of η_1 precipitates along the $[110]_{Al}$ and $[1\ \bar{1}\ 0]_{Al}$ directions, respectively, confirming the hexagonal pillar-like 3-D structure. Consistency with previous reports [30,33] was verified through fast Fourier transformation from STEM images (Fig. 1(a) and (b)), alongside observed segregation layers near the interface, aligning with earlier findings [30, 33]. Significantly, V-shaped periodic interfacial segregation layers, marked by the white dotted lines and arrows in Fig. 1(a) and (c), were observed, and the presence of nine aluminum atomic columns between these V-shaped layers was noted. This was contrary to our expectations of ten aluminum atomic columns, considering the interplanar distance of η_1 and Al, in the absence of the special periodic interface segregation layers (Fig. 1(d)). Although these special structures have been previously reported as sub-unit structures [30], their detailed atomic structure and formation have not been demonstrated. Therefore, we attempted to elucidate the atomic structures of these sub-units.

Atomic-scale EDS analysis was utilized to delineate the composition of the segregation layer at the Al/η_1 precipitate interface, as shown in Fig. 2(a)–(f). The delineation within these figures, indicated by white lines, identifies the sub-unit structure while the magnesium, aluminum, and zinc elements are depicted in green, blue and red, respectively. The EDS analysis revealed that magnesuim and zinc atoms were predominantly segregated near the aluminum/η_1 interface (Fig. 2(d)–(f)). Furthermore, the sub-unit structure was mainly composed of magnesium and zinc atoms, similar with interface segregation layer. These observations, coupled with the precipitate's hexagonal pillar morphology, led to the definitive conclusion that both the interfacial segregation layer and the sub-unit structure predominantly consist of magnesium and zinc atoms. These compositional insights facilitated the development of an atomic model, incorporating both the sub-unit structure and the interface segregation layer, through first-principles calculations.

Through a synthesis of experimental observations and first-principles calculations, we identified the most energetically stable model among the candidates presented in Supplementary Figs. 1 and 2, detailed in Fig. 3(a) and (b). These figures illustrate the schematic diagrams of the

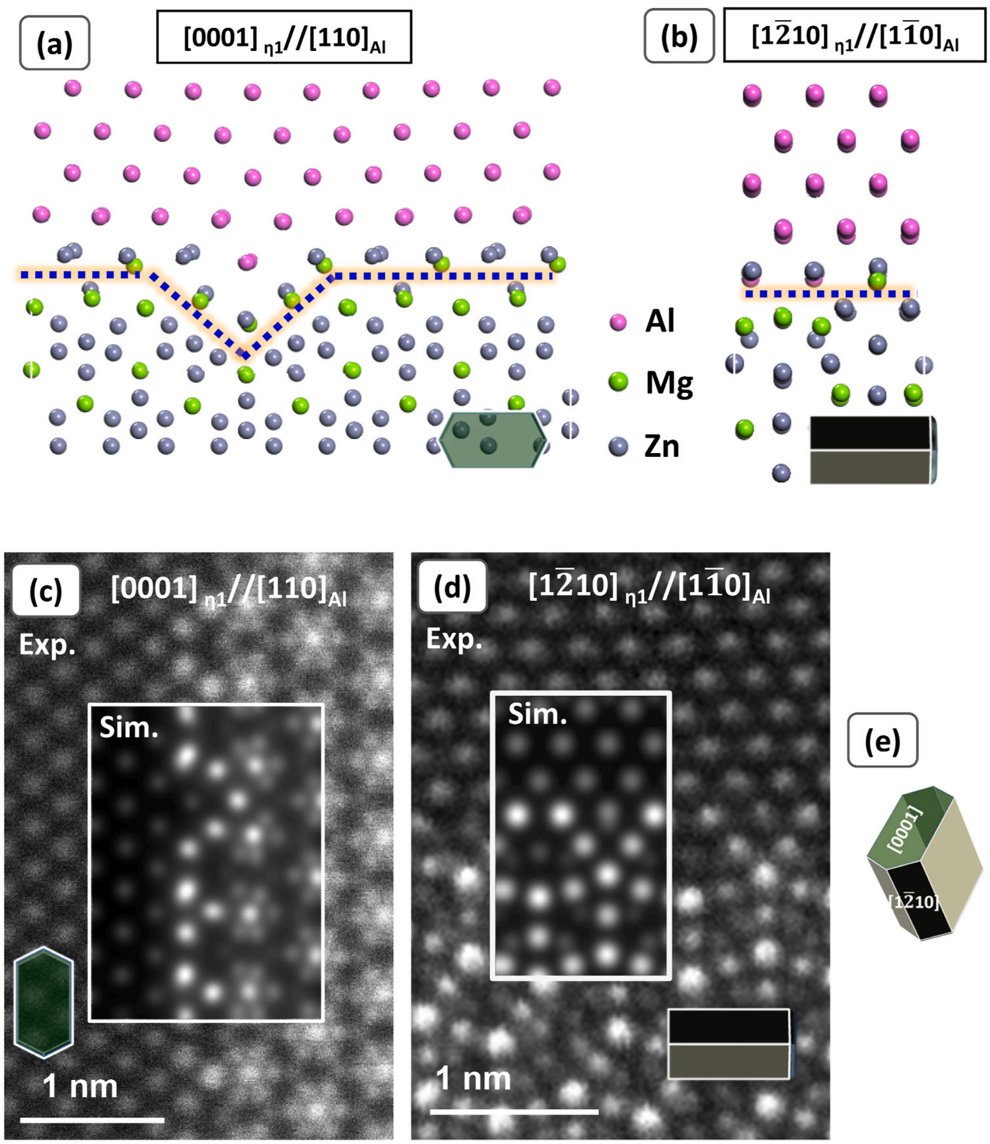

Fig. 3. (a), (b) Schematic image of the atomic structure of η_1. (a) indicates the $[110]_{Al}//[0001]_{\eta}$ and (b) indicates $[1\ \bar{1}\ 0]_{Al}//[1\ \bar{2}\ 10]_{\eta}$. (c), (d) STEM simulation result and corresponding HAADF-STEM experiment results. (c) $[110]_{Al}//[0001]_{\eta}$ (d) $[1\ \bar{1}\ 0]_{Al}//[1\ \bar{2}\ 10]_{\eta}$. (e) Schematic diagram of 3-D morphology of η_1 and corresponding direction. Exp. stands for experimental observation results and Sim. indicates STEM simulation results. The images within the white box are STEM simulation results.

orientation relationship between $[0001]_{\eta}$ and $[110]_{Al}$ and between $[1\ \bar{2}\ 10]_{\eta}$ and $[1\ \bar{1}\ 0]_{Al}$, respectively. To assess the fidelity of our calculated model, we conducted STEM simulations based on the calculated model and compared these with the actual STEM experimental findings (Fig. 3 (c) and (d)). The results within the white square box represent the simulation outcomes, which closely overlap with the experimental results. By comparing the simulation and experiment, we could identify that Aluminum atoms and η precipitate's Magnesium and Zinc atom positions are well aligned, with their Aluminum to η precipitate intensity distribution is separated distinctively. This simulation results are in good agreement with the previously reported in the literature [33]. Consequently, our simulation results not only closely aligned with experimental observations but also correspond with findings previously documented in the literature, which means that the calculated model is a suitable representative of these sub-unit structures.

3.2. Origin of sub-unit structure formation at the interface

In our investigation into the formation of sub-unit structures, we initially anticipated the development of a planar interface between the precipitate and matrix, as illustrated in Fig. 4(a), due to its potential to minimize interface area. Contrary to expectations, both our experimental findings and previous studies [30] reveal the emergence of sub-unit structures. This observation leads us to conclude that sub-unit structures are energetically more favorable than their planar counterparts, owing to their lower interfacial energy per unit area. This indicates a significant stability advantage for precipitates exhibiting sub-unit structures over those with planar interfaces. The interfacial energy comprises two components: chemical and structural. The chemical contribution is derived from the difference in chemical components, whereas the structural contribution arises from structural distortions, such as strained structures, dislocations, and volume misfits. Aluminum/η_1 interface is incoherent structure, which has much higher structural contribution than chemical contribution [39]. Moreover, the chemical composition is similar at both interface layers, the planar interface model (Fig. 4(a)) and the interface model having sub-unit structure (Fig. 4(b)), we focused on the difference in the structural contribution of those two structural models.

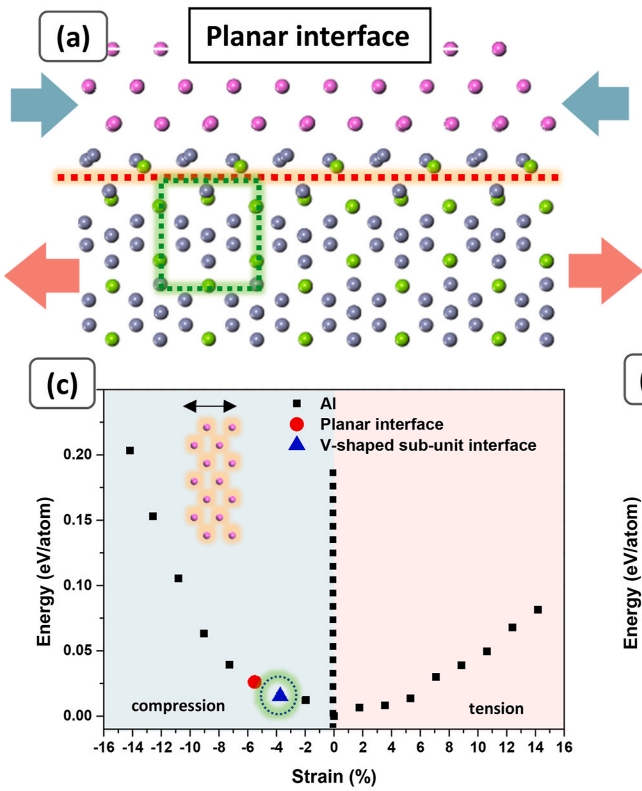

Fig. 4. (a) Schematic atomic structure of planar interface model. (b) Schematic atomic structure of sub-unit interface structure model. (c) Calculated strain energy of Al along $[1\ \overline{1}\ 0]_{Al}$. (d) Calculated strain energy of η_1 along $[1\ \overline{2}\ 10]_{\eta}$. Red circle represents planar interface model and blue triangle demonstrates sub-unit interface structure model. (For interpretation of the references to color in this figure legend, the reader is referred to the Web version of this article.)

Table 1
Strain of matrix and precipitate from each interface model.

	Strain of Planar interface (%)	Strain of Sub-unit interface (%)
Al	−5.494	−3.722
$MgZn_2$ (η)	5.961	−1.987

Table 2
Strain energy of matrix and precipitate from each interface model.

	Strain energy of Planar interface (eV/atom)	Strain energy of Sub-unit interface (eV/atom)
Al	0.0217	0.0151
$MgZn_2$ (η)	0.0261	0.0038

We now highlight the key differences between the two models. Unlike the uniformity of the planar interface model, the sub-unit interface model introduces a periodic V-shaped pattern, emerging every five precipitate units – a feature distinctly marked in Fig. 1(c), (d), and 4(a) with green dotted box. This model effectively integrates the predictability of the planar interface with the recurrent V-shaped sub-units, underscoring its unique periodicity. In comparing both models, it was observed that while the planar interface model necessitates ten aluminum atomic pillars per five precipitate unit structures, the sub-unit interface model efficiently requires only nine. This discrepancy suggests that the planar interface between aluminum and η_1 induces significant strain along the $[1\ \overline{1}\ 0]_{Al}$ direction, evidenced by a 10% lattice misfit difference between aluminum and η_1 precipitates. To quantify this, strain energy was evaluated by comparing the most stable states of Al and η_1 in both models, revealing a reduction in strain with the sub-unit interface model (Table 1). From Table 1, we could identify that strain of both Al and η was decreased with formation of sub-unit interface. This was corroborated by first-principles calculations, changing the supercell size of Al along the $[1\ \overline{1}\ 0]_{Al}$ and η along $[1\ \overline{2}\ 10]_{\eta}$. We compared the strain energies of the aluminum matrix in the planar and sub-unit interface models from an energetic perspective utilizing first-principles calculations for a detailed energetic analysis (Fig. 4(c)). The quantitative strain energy values, presented in Table 2, show that the sub-unit interface structure model incurs lower strain energy within the aluminum matrix compared to the planar interface model. Furthermore, an analogous comparison of the η_1 precipitate's strain energy across both interface models, as illustrated in Fig. 4(a) and (b), and summarized in Fig. 4(d), reinforces the conclusion that the sub-unit interface structure model is energetically more favorable. These findings collectively indicate that the role of sub-unit interface structure in mitigating strain relaxation of both the aluminum matrix and the η_1 precipitates, thereby elucidating their contribution to the enhanced stability of the system.

To substantiate the strain energy calculations, we implemented a geometrical phase analysis using the atomic-scale image of η_1 and Al (Fig. 5(a)). The boxes outlined in colored dotted lines in the image served as the reference area of the aluminum matrix and η_1 precipitate. Given the computed strain values of about −4 % of aluminum and −2 % for the η_1 precipitate from the sub-unit interface structure model, we accordingly adjusted the colorbar scale to reflect these thresholds. Strains exceeding these limits were vividly highlighted in red or blue color. Observations revealed that the strain within aluminum matrix (Fig. 5(b)) predominantly remained within ±4% range, while the η_1 precipitate strain (Fig. 5(c)) stayed below ±2%, barring the upper precipitate region. Therefore, we can conclude that the formation of the sub-unit interface structure in η_1/aluminum facilitates the simultaneous strain relaxation of both the aluminum matrix and η_1 precipitate.

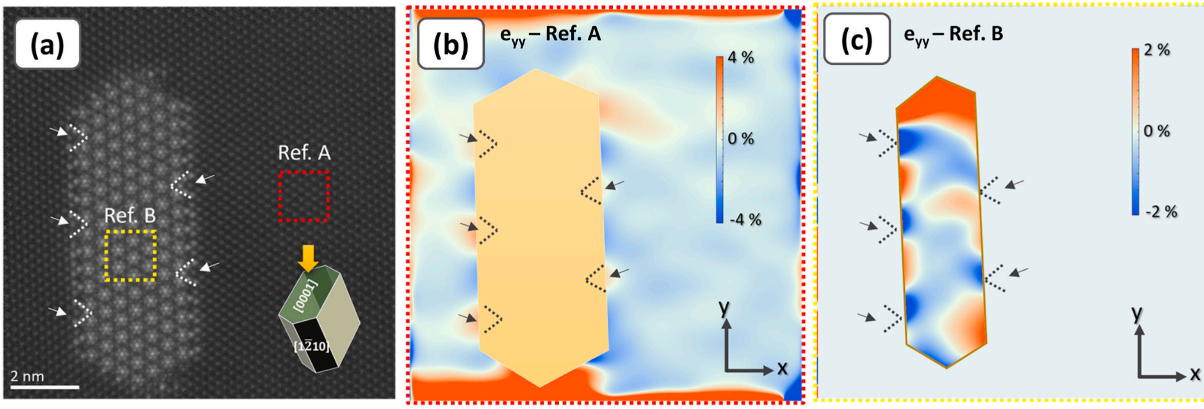

Fig. 5. (a)–(c) HAADF-STEM image and corresponding GPA images. (b) Strain map of Al along $[1\ \bar{1}\ 0]_{Al}$. Reference area is indicated in (a) with red dotted box. (c) Strain map of η along $[1\ \bar{2}\ 10]_{\eta}$. Reference area is shown in (a) with yellow dotted box. (For interpretation of the references to color in this figure legend, the reader is referred to the Web version of this article.)

4. Conclusions

In this study, we explored the interface structure of the η_1/aluminum system, focusing on the novel V-shaped sub-unit interface structure through STEM and DFT analyses. The comparison between models with and without the sub-unit structure highlighted that incorporating the sub-unit interface structure reduces the need for aluminum matrix atomic columns, enhancing system stability by facilitating strain relaxation in both the aluminum matrix and η_1 precipitates. These findings offer valuable insights into the design and development of novel materials with enhanced mechanical properties, which are essential for enhancing the performance of advanced materials.

Declaration of competing interest

The authors declare that they have no known competing financial interests or personal relationships that could have appeared to influence the work reported in this paper.

Acknowledgements

This study was supported by National Research Foundation of Korea (NRF) grants funded by the Korean Government (MSIT) (NRF-2021R1A2C3005096, NRF-2021M3H4A6A01045764, NRF-2019M3D1A1079215, and NRF-2022R1A2C1005505). The Institute of Engineering Research at Seoul National University provided research facilities for this work.

Appendix A. Supplementary data

Supplementary data to this article can be found online at https://doi.org/10.1016/j.jmrt.2024.03.012.

References

[1] Xin T, Zhao Y, Mahjoub R, Jiang J, Yadav A, Nomoto K, et al. Ultrahigh specific strength in a magnesium alloy strengthened by spinodal decomposition. Sci Adv 2021;7:1–9. https://doi.org/10.1126/SCIADV.ABF3039/SUPPL_FILE/ABF3039_SM.PDF.

[2] Yang W, Luo ZP, Bao WK, Xie H, You ZS, Jin HJ. Light, strong, and stable nanoporous aluminium with native oxide shell. Sci Adv 2021;7:1–10. https://doi.org/10.1126/SCIADV.ABB9471/SUPPL_FILE/ABB9471_SM.PDF.

[3] Ganesh MRS, Reghunath N, Levin M J, Prasad A, Doondi S, Shankar KV. Strontium in Al–Si–Mg alloy: a review. Met Mater Int 2022;28:1–40. https://doi.org/10.1007/S12540-021-01054-Y/FIGURES/54.

[4] Deng S, Zhao H, Li R, Shao J, Li J, Qi L, et al. Composition design of low hot-cracking susceptibility of Al-Zn-Mg-Sc alloy and its formability during laser additive manufacturing. Mater Char 2022;193:112304. https://doi.org/10.1016/J.MATCHAR.2022.112304.

[5] Shen G, Chen X, Yan J, Fan L, Yang Z, Zhang J, et al. Effects of heat treatment processes on the mechanical properties, microstructure evolution, and strengthening mechanisms of Al–Mg–Zn–Cu alloy. J Mater Res Technol 2023;27:5380–8. https://doi.org/10.1016/J.JMRT.2023.11.070.

[6] Zhao Y, Tian T, Jia H, Ma P, Yang Z, Xu J, et al. Effects of Mg/Zn ratio and pre-aging on microstructure and mechanical properties of Al–Mg–Zn–Cu alloys. J Mater Res Technol 2023;27:1874–85. https://doi.org/10.1016/J.JMRT.2023.09.319.

[7] Kshetri R, Ajay. Heat flux and heat transfer coefficient model analysis during turning of al (7068) alloy. Mater Today Proc 2021;46:6757–69. https://doi.org/10.1016/J.MATPR.2021.04.299.

[8] Hansen V, Karlsen OB, Langsrud Y, Gjønnes J. Precipitates, zones and transitions during aging of Al-Zn-Mg-Zr 7000 series alloy. Mater Sci Technol 2004;20:185–93. https://doi.org/10.1179/026708304225010424.

[9] Löffler H, Kovács I, Lendvai J. Decomposition processes in Al-Zn-Mg alloys. J Mater Sci 1983;18:2215–40. https://doi.org/10.1007/BF00541825/METRICS.

[10] Chung T-F, Yang Y-L, Huang B-M, Shi Z, Lin J, Ohmura T, et al. Transmission electron microscopy investigation of separated nucleation and in-situ nucleation in AA7050 aluminium alloy. Acta Mater 2018;149:377–87. https://doi.org/10.1016/j.actamat.2018.02.045.

[11] Nie JF. Physical metallurgy of light alloys. Physical Metallurgy: Fifth Edition 2014;1:2009–156. https://doi.org/10.1016/B978-0-444-53770-6.00020-4.

[12] Sha G, Cerezo A. Early-stage precipitation in Al–Zn–Mg–Cu alloy (7050). Acta Mater 2004;52:4503–16. https://doi.org/10.1016/J.ACTAMAT.2004.06.025.

[13] Marioara CD, Lefebvre W, Andersen SJ, Friis J. Atomic structure of hardening precipitates in an Al-Mg-Zn-Cu alloy determined by HAADF-STEM and first-principles calculations: relation to η-MgZn2. J Mater Sci 2013;48:3638–51. https://doi.org/10.1007/S10853-013-7158-3/TABLES/3.

[14] Berg LK, Gjoønnes J, Hansen V, Li XZ, Knutson-Wedel M, Waterloo G, et al. GP-zones in Al–Zn–Mg alloys and their role in artificial aging. Acta Mater 2001;49:3443–51. https://doi.org/10.1016/S1359-6454(01)00251-8.

[15] Liu JZ, Chen JH, Liu ZR, Wu CL. Fine precipitation scenarios of AlZnMg(Cu) alloys revealed by advanced atomic-resolution electron microscopy study Part II: fine precipitation scenarios in AlZnMg(Cu) alloys. Mater Char 2015;99:142–9. https://doi.org/10.1016/J.MATCHAR.2014.11.027.

[16] Liu JZ, Chen JH, Yang XB, Ren S, Wu CL, Xu HY, et al. Revisiting the precipitation sequence in Al–Zn–Mg-based alloys by high-resolution transmission electron microscopy. Scripta Mater 2010;63:1061–4. https://doi.org/10.1016/J.SCRIPTAMAT.2010.08.001.

[17] Maloney SK, Hono K, Polmear IJ, Ringer SP. The chemistry of precipitates in an aged Al-2.1Zn-1.7Mg at.% alloy. Scripta Mater 1999;41:1031–8. https://doi.org/10.1016/S1359-6462(99)00253-5.

[18] Mukhopadhyay AK, Yang QB, Singh SR. The influence of zirconium on the early stages of aging of a ternary Al-Zn-Mg alloy. Acta Metall Mater 1994;42:3083–91. https://doi.org/10.1016/0956-7151(94)90406-5.

[19] Chatterjee A, Qi L, Misra A. In situ transmission electron microscopy investigation of nucleation of GP zones under natural aging in Al-Zn-Mg alloy. Scripta Mater 2022;207:114319. https://doi.org/10.1016/J.SCRIPTAMAT.2021.114319.

[20] Kverneland A, Hansen V, Vincent R, Gjønnes K, Gjønnes J. Structure analysis of embedded nano-sized particles by precession electron diffraction. η′-precipitate in an Al–Zn–Mg alloy as example. Ultramicroscopy 2006;106:492–502. https://doi.org/10.1016/J.ULTRAMIC.2006.01.009.

[21] Kverneland A, Hansen V, Thorkildsen G, Larsen HB, Pattison P, Li XZ, et al. Transformations and structures in the Al–Zn–Mg alloy system: a diffraction study using synchrotron radiation and electron precession. Mater Sci Eng, A 2011;528:880–7. https://doi.org/10.1016/J.MSEA.2010.10.001.

[22] Gjønnes J, ChrJ Simensen. An electron microscope investigation of the microstructure in an aluminium-zinc-magnesium alloy. Acta Metall 1970;18:881–90. https://doi.org/10.1016/0001-6160(70)90016-7.

[23] Yang W, Ji S, Wang M, Li Z. Precipitation behaviour of Al–Zn–Mg–Cu alloy and diffraction analysis from η′ precipitates in four variants. J Alloys Compd 2014;610: 623–9. https://doi.org/10.1016/J.JALLCOM.2014.05.061.
[24] Li XZ, Hansen V, GjØnnes J, Wallenberg LR. HREM study and structure modeling of the η′ phase, the hardening precipitates in commercial Al–Zn–Mg alloys. Acta Mater 1999;47:2651–9. https://doi.org/10.1016/S1359-6454(99)00138-X.
[25] Chung T-F, Yang Y-L, Tai C-L, Shiojiri M, Hsiao C-N, Tsao C-S, et al. HR-STEM investigation of atomic lattice defects in different types of η precipitates in creep-age forming Al–Zn–Mg–Cu aluminium alloy. Mater Sci Eng, A 2021;815:141213. https://doi.org/10.1016/j.msea.2021.141213.
[26] Bendo A, Matsuda K, Lervik A, Tsuru T, Nishimura K, Nunomura N, et al. An unreported precipitate orientation relationship in Al-Zn-Mg based alloys. Mater Char 2019;158:109958. https://doi.org/10.1016/j.matchar.2019.109958.
[27] Godard D, Archambault P, Aeby-Gautier E, Lapasset G. Precipitation sequences during quenching of the AA 7010 alloy. Acta Mater 2002;50:2319–29. https://doi.org/10.1016/S1359-6454(02)00063-0.
[28] Chung T-F, Yang Y-L, Shiojiri M, Hsiao C-N, Li W-C, Tsao C-S, et al. An atomic scale structural investigation of nanometre-sized η precipitates in the 7050 aluminium alloy. Acta Mater 2019;174:351–68. https://doi.org/10.1016/j.actamat.2019.05.041.
[29] Lervik A, Marioara CD, Kadanik M, Walmsley JC, Milkereit B, Holmestad R. Precipitation in an extruded AA7003 aluminium alloy: observations of 6xxx-type hardening phases. Mater Des 2020;186:108204. https://doi.org/10.1016/J.MATDES.2019.108204.
[30] Ou Y, Jiang Y, Wang Y, Liu Z, Lervik A, Holmestad R. Vacancy and solute co-segregated η1 interface in over-aged Al-Zn-Mg alloys. Acta Mater 2021;218: 117082. https://doi.org/10.1016/j.actamat.2021.117082.
[31] Barker B. The effect of certain trace-element additions on the aging behavior of an aluminum-4 Wt percent Zn-3 Wt percent magnesium alloy. J Aust Inst Met 1972; 17:31–8.
[32] Ryum N. Precipitation kinetics in an Al-Zn-Mg-alloy. Int J Mater Res 1975;66: 338–43. https://doi.org/10.1515/ijmr-1975-660603.
[33] Cheng B, Zhao X, Zhang Y, Chen H, Polmear I, Nie J-F. Co-segregation of Mg and Zn atoms at the planar η1-precipitate/Al matrix interface in an aged Al–Zn–Mg alloy. Scripta Mater 2020;185:51–5. https://doi.org/10.1016/j.scriptamat.2020.04.004.
[34] Kim H, Choi H, Oh J, Lee S, Kwon H, Park ES, et al. Elucidating the role of a unique step-like interfacial structure of η4 precipitates in Al-Zn-Mg alloy. Sci Adv 2023;9: 1–9. https://doi.org/10.1126/SCIADV.ADF7426/SUPPL_FILE/SCIADV.ADF7426_SM.PDF.
[35] Kim Hwangsun. Atomic-scale structure analysis of η-precipitates. In: Al-Zn-Mg alloy. Seoul National University; 2022.
[36] Tsuru T, Yamaguchi M, Ebihara K, Itakura M, Shiihara Y, Matsuda K, et al. First-principles study of hydrogen segregation at the MgZn2 precipitate in Al-Mg-Zn alloys. Comput Mater Sci 2018;148:301–6. https://doi.org/10.1016/j.commatsci.2018.03.009.
[37] Tsuru T, Shimizu K, Yamaguchi M, Itakura M, Ebihara K, Bendo A, et al. Hydrogen-accelerated spontaneous microcracking in high-strength aluminium alloys. Sci Rep 2020;10:1998. https://doi.org/10.1038/s41598-020-58834-6.
[38] Barthel J. Dr. Probe: a software for high-resolution STEM image simulation. Ultramicroscopy 2018;193:1–11. https://doi.org/10.1016/j.ultramic.2018.06.003.
[39] Porter DA, Easterling KE. Phase transformations in metals and alloys (revised reprint). CRC press; 2009.